Enhanced Crystal Growth in Binary Lennard-Jones Mixtures

M. Radu* and K. Kremer†
Max-Planck Institut für Polymerforschung, Ackermannweg 10, D-55128 Mainz, Germany
(Received 21 September 2016; revised manuscript received 2 November 2016; published 31 January 2017)

We study the crystal growth in binary Lennard-Jones mixtures by molecular dynamics simulations. Growth dynamics, the structure of the liquid-solid interfaces as well as droplet incorporation into the crystal vary with solution properties. For demixed systems we observe a strongly enhanced crystal growth at the cost of enclosed impurities. Furthermore, we find different interface morphologies depending on solubility. We relate our observations to growth mechanisms based on the Gibbs-Thomson effect as well as to predictions of the Kardar-Parisi-Zhang theory in $2+1$ dimensions.

DOI: 10.1103/PhysRevLett.118.055702

Additive modified crystallization—i.e., nucleation and crystal growth under the influence of process promoting or inhibiting additional substances—is common in nature, e.g., during the growth of calcitic stalactites, of mollusk shells or of bone structures [1–5]. Modification of nucleation and growth either appears by variation of thermodynamic conditions like component miscibility within solution [6,7], or by the addition of stimuli-responsive (macro-) molecules [8–10]. Several modification routes for crystallization processes in model systems like calcium carbonates have been studied. A variety of different impact ways is proposed, which rely on both the properties of the crystallizing material as well as on the additives used, such as polymer and/or surface functionalization [11,12], adsorption preferences [13], solute and additive concentration [14]. Regulating the formation of crystalline structures by additives is already playing an important role in, e.g., the pharmaceutical industry [15,16], fuel production [17], or the fabrication of glass ceramics [18]. However, a microscopic control and analysis of these nonequilibrium processes only recently drew the attention of various studies. ten Wolde and Frenkel verified the existence of conceptual differences in crystallization pathways of model proteins between systems at the critical temperature T_c for liquid-liquid phase separation or right below [19]. At T_c critical density fluctuations, acting as nucleation sites, tend to decrease the free energy barrier for crystal nucleation. By that they increase the crystallization rate compared to slightly undercooled samples. In the following years, this mode of crystallization was studied further by means of simulations as well as experiments [20–25]. Mosses *et al.* [26] adopted this concept for water crystallization in *trans*-DCE close to the liquid-liquid critical point. There the authors were able to template growing ice crystals, but only in an irregular and uncontrollable way. They also studied hexane in nitrobenzene, where the nitrobenzene rich fraction can crystallize in an irregular way below the liquid-liquid binodal. In general, studies on the interplay of demixing and crystallization span various fields of current research like, e.g., polymer science [27] or crystallization phenomena in metal alloys [28].

Instead of focusing on a specific system (together with a specific path of tuning crystallization), we here shed light on more general effects that are inherent in these additive modified processes. To do so, we investigate generic effects in crystal growth dynamics. We modify growth process by (i) adding a second, not crystallizing particle species to the system and (ii) alter the thermodynamic properties of the solution from miscible to segregating in supersaturated binary Lennard-Jones (LJ) samples. For simple systems like this Koschke *et al.* [29] recently showed that even small amounts of additives can shift the onset of crystallization, an effect known as freezing point depression [30–32], compared to pure solvent systems. Here a particular interplay between the evolution of the bulk crystal and of the liquid-solid interface (IF) is found, regulating the overall growth dynamics and crystal shape. Obtained results can be related to the *vapor-liquid-solid* mechanism [33,34], where anisotropic crystal growth occurs in the presence of a crystal-vapor and a crystal-liquid interface. Furthermore, the evolution of the IF width can be linked to the theoretical framework of Kardar, Parisi, and Zhang (KPZ) [35], i.e., the description of growth processes in terms of stochastic differential equations.

The mixtures were studied by molecular dynamics (MD) simulations and consist of the two particle species A and B with a fixed B particle mole fraction of $f_B = 0.8$. A crystalline slab of B particles was inserted at the beginning of the simulation. The two surfaces of the slab resembled [1, 0, 0] fcc plane structures. When crystal growth processes are studied in finite systems the growth conditions change as soon as depletion effects set in Ref. [36]. Then the previously constant chemical potential difference $\Delta\mu$ for B particles being in the solid or in the liquid state—and by this the force which drives the transition—changes as it depends on f_B. As a result it is desirable to use a simulation procedure which maintains f_B in the vicinity of the IF. In contrast to grand canonical simulation methods

[37] (which require an adaptive-resolution scheme [38] for dense systems), here, a modified version of the constant chemical potential MD (CμMD) method of Perego *et al.* [36], is used.

The miscibility of A and B particles in solution is varied in terms of the ϵ parameter for the A-B interaction; i.e., large values of ϵ_{AB} represent systems of good solubility while for small but positive ϵ_{AB} the solutions tend to demix. For each value of ϵ_{AB} 8 independent simulation runs were performed. Interaction parameters chosen are $\sigma_{AA} = 1.0$, $\sigma_{BB} = 1.1765$, $\epsilon_{AA} = 1.0$, and $\epsilon_{BB} = 1.6$, respectively, and $\sigma_{AB} = (\sigma_{AA} + \sigma_{BB})/2 = 1.0882$. The MD simulations were performed using the ESPResSo++ simulation package [39]. Snapshots were prepared with the OVITO visualization tool [40]. For more details on the simulation setup and parameter definitions see the Supplemental Material [41]. Here, ϵ_{AB} was always chosen to be below the geometric mean of $\epsilon_{AB}^{\text{mix}} := \sqrt{\epsilon_{AA}\epsilon_{BB}}$ and is varied from 0.2ϵ to 1.2ϵ. For these interaction values binary LJ mixtures were found to be within the liquid-solid coexistence region [47] and contain a liquid A particle rich and a solid B particle rich phase, respectively. Accordingly, A particles stay in the liquid state throughout the simulation while B particles crystallize. In comparison, the corresponding pure B particle system is supercooled and tends to crystallize [48]. In case of ϵ_{AB} approaching $\sqrt{\epsilon_{AA}\epsilon_{BB}}$ type-specific particle affinities vanish, cf. snapshot for $\epsilon_{AB} = 1.2\epsilon$—referred to as *good* solubility—in Fig. 1. In contrast, by decreasing ϵ_{AB}, both particle species tend to demix. As a result, a liquid-liquid phase separation was observed during which droplets of A particles were formed, as illustrated in Fig. 1 for $\epsilon_{AB} = 0.2\epsilon$ (entitled as *poor* solubility).

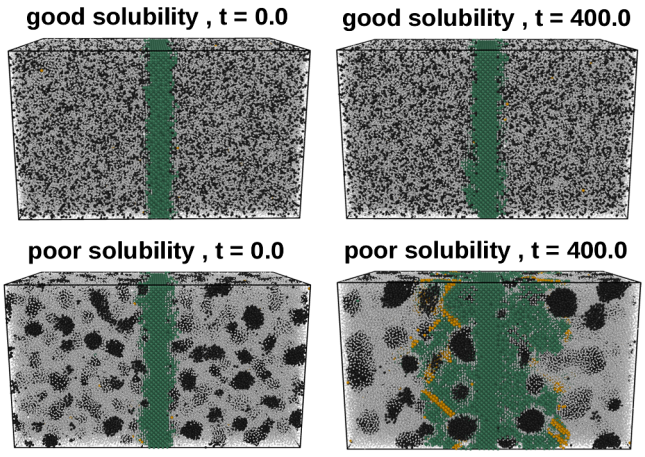

FIG. 1. Snapshots of simulation boxes for systems of good (upper panel) and poor solubility (lower panel). Particle species in the liquid state are shown in black, and light gray for the A and B particles, respectively, while crystalline B particles are dark green for fcc- and orange for hcp-like structures, each of which was determined according to the Steinhardt order parameter [49] (cf. Supplemental Material [41]). The figure depicts configurations obtained at different points in time.

Figure 2 shows the overall crystal growth dynamics of $N_X(t)/N_X(0)$ B particles (fcc as well as hcp) $N_X(t)/N_X(0)$ in the crystallite with respect to its initial value at $t = 0\tau$. While the monatomic system displays a linear growth in time (see also Refs. [50,51]), binary mixtures can be related to two different types of growth scenarios. For values of $\epsilon_{AB} \geq 1.0\epsilon$, not far below $\epsilon_{AB}^{\text{mix}}$ N_X increases, but only very slowly. There the tendency to phase segregation still is very weak and the crystallizing component is effectively diluted. Even more so, since A particles are (almost) not incorporated in the crystal, close to the crystal surface a B particle depletion zone is formed. Altogether this results in the observed slow crystal growth shown by comparing the snapshots of Fig. 1. Decreasing the A-B interaction parameter to $\epsilon_{AB} \leq 0.8\epsilon$ changes the situation drastically to the opposite. In this regime the growth of the crystallites experience an acceleration indicated by the curves bending away from linear to (intermediately) faster than linear growth in Fig. 2.

As mentioned before, demixing of the solution leads to the formation of A particle droplets. The lower panel of Fig. 1 shows how these droplets modulate the IF structure and get incorporated into the crystal. Furthermore, planar defects in the form of hcp structured crystalline layers occur (which will be investigated systematically in another study). The resulting height variation is shown in Fig. 3. Panel (a) shows top views of typical IFs for the highest and lowest studied ϵ_{AB} of 1.2ϵ (left) and 0.2ϵ (right). While the IF is almost flat in the case of good solubility, for the phase separated system a pronounced roughness across the IF is visible. The IF modulations due to the presence of A droplets furthermore cause spatial variations in the local IF growth velocity as shown in panel (b) of the same figure. While particle incorporation at crystallite regions covered by droplets is inhibited, above free crystalline sites the growth becomes accelerated as long as the active IF growth continues. Two reasons can be identified for this acceleration. First the phase segregation locally leads to a higher

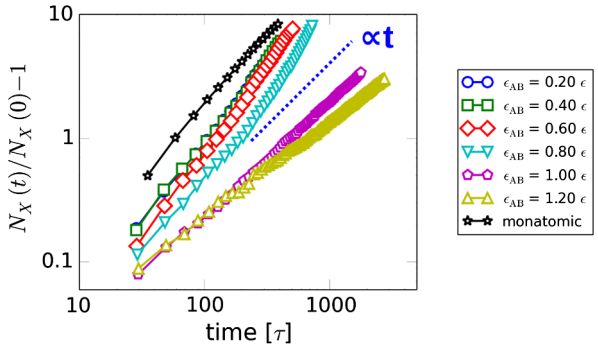

FIG. 2. Number of crystalline particles within the growing crystallite normalized to its initial value as a function of time. Curves are shown for ϵ_{AB} between 0.2ϵ and 1.2ϵ as well as for a monatomic system. Data for 0.2ϵ and 0.4ϵ are almost indistinguishable. Linear behavior is depicted by the dashed blue line.

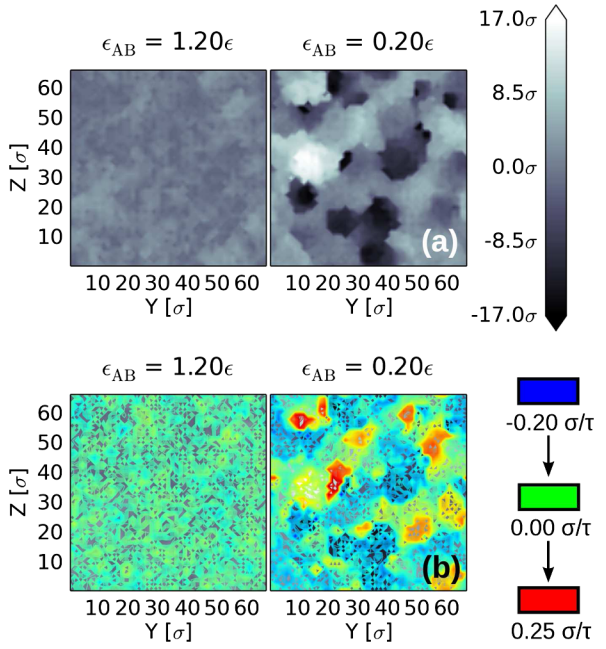

FIG. 3. (a) Color maps of typical crystal height fields with respect to the mean of the IF at $t = 400\tau$. Color measures the local crystal height $h(\mathbf{x})$—where $\mathbf{x} := (y, z)$—above the planar crystalline substrate with respect to its mean value $\langle h(\mathbf{x})\rangle$. (b) Scans of local crystal growth velocities with respect to the mean rates of $1.8 \times 10^{-3}\sigma/\tau$ for 1.2ϵ and $6.8 \times 10^{-2}\sigma/\tau$ for 0.2ϵ according to the IFs shown in (a). The color coding reflects respective values between $-0.20\sigma/\tau$ and $0.25\sigma/\tau$.

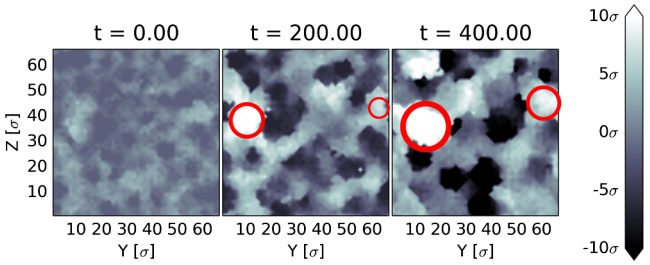

FIG. 4. Scans depicting the temporal evolution of the crystal heights for a system with $\epsilon_{AB} = 0.2\epsilon$. Here, the value 0.00σ refers to the mean IFs. Red circles mark crystalline structures that grow around the A particle droplet inclusions and whose lateral dimensions increase as a function of time.

B particle concentration compared to the overall mixture. Thus we expect a growth rate approaching that of the pure B system. Segregation induced roughness leads to a second cause of accelerated growth. This roughness produces more surface exposed to the liquid and thus more growth. Following the Gibbs-Thomson effect [52–54], which describes the origin of Ostwald ripening, the surface should flatten again, locally displaying the pure B-system growth. This, however is limited, or at least delayed, by the presence of liquid A droplets, which determine a characteristic length scale for the roughness. Consequently, this allows the conjecture that the growth rate of the mixed system, which eventually will become linear in time, might asymptotically indeed be faster than for a pure B-particle system, provided one is not yet in the fully phase separated regime. Actually, on the time scale of the present study we could not yet observe any limitation of the accelerated growth in case of $\epsilon_{AB} \leq 0.8\epsilon$ (cf. 2). Thus $N_X(t)$ might as well cross the $N_X(t)$ line for monatomic systems when studying larger simulation boxes and longer times. Systematic future investigations of (possible collective) particle dynamics, e.g., Ref. [55] should reveal more details, but are beyond the scope of this Letter.

To shed more light on the IF roughness the case $\epsilon_{AB} = 0.2\epsilon$ is illustrated in Fig. 4. From left to right the scans show the time dependence of the IF roughness. Red circles mark fast growing structures of increasing diameter. Those are separated by likewise growing A particle droplets, whose growth dynamics is quantified by the respective static structure factors (SSFs) [56] (see Supplemental Material [41]). Panel (a) of Fig. 5 depicts droplet radii R_g as a function of ϵ_{AB} (increasing solubility from left to right) and compares the data for two different points in time. Initially ($t = 0\tau$, blue circles) the data for $\epsilon_{AB} \leq 0.8\epsilon$ reflect the presence of A particle droplets with average radii of gyration between 1.8σ and 3.1σ. In contrast, i.e., for the cases of $\epsilon_{AB} \geq 1.0\epsilon$, A particles are almost totally dispersed in solution. As time moves on, for $\epsilon_{AB} \leq 0.8\epsilon$, droplets

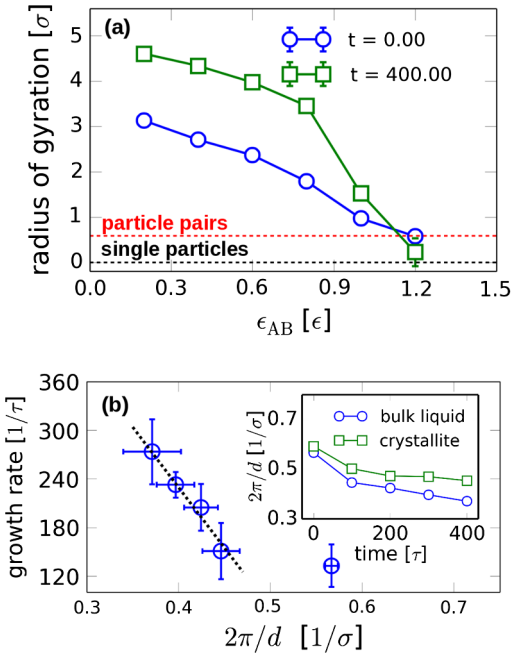

FIG. 5. Properties of the A particle droplets in the bulk liquid. (a) Radius of gyration of droplets as a function of ϵ_{AB} for two subsequent points in time. (b) Growth rate for $\epsilon_{AB} = 0.2\epsilon$ against the inverse of the average distance between droplets $1/d$. Inset: $1/d$ versus time for A particle droplets located in the bulk liquid and within the crystallite, respectively.

continue to grow due to preference to demix the systems. However, for miscible solutions (i.e., $\epsilon_{AB} \geq 1.0\epsilon$), droplets hardly grow at all, as seen at a later stage of the simulation run ($t = 400\tau$, green squares). At the same time the mean distance between these droplets d also increases in a way that depends on the droplet location perpendicular to crystalline substrate. In contrast to droplets in the bulk liquid, where $1/d$ continues to decrease, those incorporated into the crystallite are stuck both in size and arrangement, cf. inset of Fig. 5(b), due to the aforementioned caging effect. According to the Gibbs-Thompson scheme coarsening of the droplets should lead to an increased growth rate, if the effect of reduction of the available crystal surface is not more important. In Fig. 5(b) the crystal growth rate as a measure of the chemical potential difference $\Delta\mu$ is plotted against $1/d$. The results reflect the expected linearly decreasing behavior (black dotted line) up to a value of the inverse droplet separation at $t = 0.0\tau$, i.e., before distinguished IF structures according to Fig. 4 occurred.

As we have seen above, the growth of the crystallites is strongly related to the structural evolution of the IF. In contrast to the heterogeneously growing crystalline structures of the previous paragraph, for miscible systems with $\epsilon_{AB} \geq 1.0\epsilon$, another growth mechanism was observed. In this case, single B particles are incorporated into the crystal at random lateral positions. According to the IF scans for $\epsilon_{AB} = 1.2\epsilon$ in panels (a) and (b) of Fig. 3 this behavior leads to the progression of a rather flat crystal front. In order to quantify the varying IF structures for different ϵ_{AB}, the *roughness* of the IF at time t was measured as the standard deviation of the crystal height distribution, namely,

$$w(t) \coloneqq \sqrt{\langle h(\mathbf{x},t)^2\rangle - \langle h(\mathbf{x},t)\rangle^2}, \quad (1)$$

as shown in Fig. 6. Initially ($t < 20\tau$) the curves for all ϵ_{AB} as well as for the monatomic reference system show a qualitatively similar behavior—they increase sublinearly according to almost the same exponent. Subsequently, a time regime can be identified in which, like for the growth dynamics of the bulk crystal, the range of studied solubilities can be subdivided with respect to two growth modes. For $\epsilon_{AB} \leq 0.8\epsilon$ the increase of roughnesses speeds up dramatically. This observation is in accordance with the previously discussed growth of the crystal structures that develop in between liquid A particle droplets. On the other hand, for $\epsilon_{AB} \geq 1.0\epsilon$, the growth exponent also changes, but in a less pronounced way. Here, the crystal growth mechanism can be related to the Kardar, Parisi, and Zhang [35] equation, i.e.,

$$\partial_t h(\mathbf{x},t) = \nu\nabla^2 h(\mathbf{x},t) + \lambda[\nabla h(\mathbf{x},t)]^2 + \eta(\mathbf{x},t), \quad (2)$$

which includes a Laplace-like smoothing mechanism, a local growth velocity contribution that depends on the gradient of the field and a Gaussian noise term that reflects stochasticity with respect to space and time. The constant factors ν and λ are system (material) dependent parameters. For $2+1$ dimensions, i.e., the growth of a two-dimensional height distribution into the perpendicular direction, this equation predicts a roughness that increases in the short time regime as t^β, where $\beta = 0.24$ [57], as indicated in Fig. 6. In case of well-mixed binary systems, the results qualitatively follow this trend. Similar to the good solubility regime, the roughness in case of the monatomic samples show an increase in close accordance to the predicted exponent, but on a much smaller time scale. Afterwards, $w(t)$ levels off to a constant value due to finite size effects.

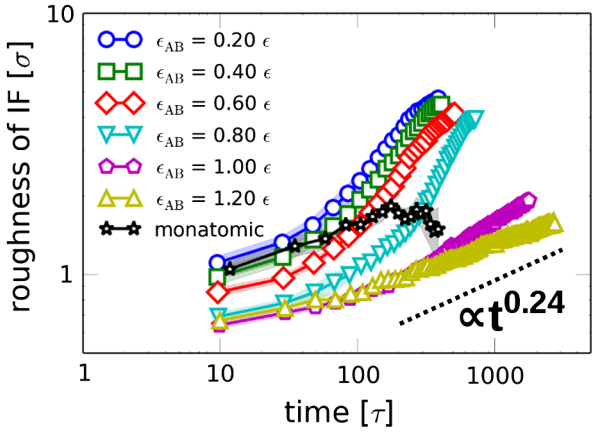

FIG. 6. IF roughness as a function of time for varying solubilities as well as the pure B particle system. The dashed black line depicts a power law for the time dependence of the roughness with an exponent $\beta = 0.24$, which follows for an intermediate time regime from the solution of the $(2+1)d$ KPZ equation [Eq. (2)].

In conclusion, our study of binary LJ mixtures in the solid-liquid coexistence regime, where one component crystallizes while the second remains in the liquid state, reveals qualitatively different means of manipulating crystal growth. For good compatibility of the components crystal growth is slowed down and the overall surface roughness stays small and can be interpreted in terms of the KPZ theory. For segregating mixtures, however, effects such as local higher concentration of crystallizing particles and finally incorporated liquid droplets of the other component, which impose significant surface roughness and Ostwald type ripening (which tends to reduce roughness), compete. Especially the latter promotes accelerated crystal growth due to surface tension effects and at the same time reduces the number of available growth sites. In qualitative agreement with the findings of Refs. [26] and [58], our results suggest the possibility of a faster crystal growth in mixed systems compared to the pure (monatomic) system for certain conditions. This will be the subject of further studies and would also be experimentally very worthwhile to investigate.

This work has been supported by the European Research Council under the European Union's Seventh Framework Programme (FP7/2007-2013)/ERC Grant Agreement No. 340906-MOLPROCOMP. We are grateful to T. Bereau for stimulating discussions, T. Stuehn for assistance with the ESPResSo++ package and B. Duenweg and T. Bereau for critical reading of the manuscript. We are also grateful to the Max Planck Computing and Data Facility (MPCDF).

*radumarc@mpip-mainz.mpg.de
†kremer@mpip-mainz.mpg.de

[1] M. Pacton, S. F. M. Breitenbach, F. A. Lechleitner, A. Vaks, C. Rollion-Bard, O. S. Gutareva, A. V. Osintcev, and C. Vasconcelos, Biogeosciences **10**, 6115 (2013).
[2] L. Addadi and S. Weiner, Angew. Chem., Int. Ed. **31**, 153 (1992).
[3] S. Weiner and L. Addadi, J. Mater. Chem. **7**, 689 (1997).
[4] S. Mann, J. Chem. Soc., Dalton Trans., 3953 (1997).
[5] F. C. Meldrum and H. Coelfen, Chem. Rev. **108**, 4332 (2008).
[6] A. Wegener, Naturwissenschaften **6**, 598 (1918).
[7] Y. Wang, A. Lomakin, R. Latypov, J. Laubach, T. Hideshima, P. Richardson, N. Munshi, K. Anderson, and G. Benedek, J. Chem. Phys. **139**, 121904 (2013).
[8] H. A. Lowenstam and S. Weiner, in *On Biomineralization* (Oxford University Press, New York, 1989).
[9] E. Baeuerlein, in *Handbook of Biomineralization: Biological Aspects and Structure Formation* (Wiley-VCH, New York, 2007).
[10] N. A. J. M. Sommerdijk and H. Coelfen, MRS Bull. **35**, 116 (2010).
[11] M. Sedlák and H. Coelfen, Macromol. Chem. Phys. **202**, 587 (2001).
[12] R. Lakshminarayanan, S. Valiyaveettil, and G. L. Loy, Cryst. Growth Des. **3**, 953 (2003).
[13] A. J. Gratz and P. E. Hillner, J. Cryst. Growth **129**, 789 (1993).
[14] A. N. Kulak, P. Iddon, Y. Li, S. P. Armes, H. Clfen, O. Paris, R. M. Wilson, and F. C. Meldrum, J. Am. Chem. Soc. **129**, 3729 (2007).
[15] C. J. Schram, S. P. Beaudoin, and L. S. Taylor, Langmuir **31**, 171 (2015).
[16] C. Schram, L. Taylor, and S. Beaudoin, Langmuir **31**, 11279 (2015).
[17] G. Knothe, Energy Fuels **22**, 1358 (2008).
[18] Y.-M. Sung, J. Mater. Sci. **31**, 5421 (1996).
[19] P. R. t. Wolde and D. Frenkel, Science **277**, 1975 (1997).
[20] J. Anwar and P. K. Boateng, J. Am. Chem. Soc. **120**, 9600 (1998).
[21] P. E. Bonnett, K. J. Carpenter, S. Dawson, and R. J. Davey, Chem. Commun. (Cambridge), 698 (2003).
[22] L. Filobelo, O. Galkin, and P. Vekilov, J. Chem. Phys. **123**, 014904 (2005).
[23] L. Xu, S. V. Buldyrev, H. E. Stanley, and G. Franzese, Phys. Rev. Lett. **109**, 095702 (2012).
[24] R. J. Davey, S. L. M. Schroeder, and J. H. terHorst, Angew. Chem., Int. Ed. Engl. **52**, 2166 (2013).
[25] A. Wallace, L. Hedges, A. F. Martinez, P. Raiteri, J. Gale, G. Waychunas, S. Whitelam, J. Banfield, and J. D. Yoreo, Science **341**, 885 (2013).
[26] J. Mosses, D. A. Turton, L. Lue, J. Sefcik, and K. Wynne, Chem. Commun. (Cambridge) **51**, 1139 (2015).
[27] H. Tanaka and T. Nishi, Phys. Rev. Lett. **55**, 1102 (1985).
[28] C. Desgranges and J. Delhommelle, J. Am. Chem. Soc. **136**, 8145 (2014).
[29] K. Koschke, H. J. Limbach, K. Kremer, and D. Donadio, Mol. Phys. **113**, 2725 (2015).
[30] R. W. Potter, M. A. Clynne, and D. L. Brown, Economic Geology **73**, 284 (1978).
[31] H. K. Christenson, J. Phys. Condens. Matter **13**, R95 (2001).
[32] K. D. Collins, G. W. Neilson, and J. E. Enderby, Biophys. Chem. **128**, 95 (2007).
[33] R. S. Wagner and W. C. Ellis, Appl. Phys. Lett. **4**, 89 (1964).
[34] E. Givargizov, J. Cryst. Growth **31**, 20 (1975).
[35] M. Kardar, G. Parisi, and Y.-C. Zhang, Phys. Rev. Lett. **56**, 889 (1986).
[36] C. Perego, M. Salvalaglio, and M. Parrinello, J. Chem. Phys. **142**, 144113 (2015).
[37] D. Frenkel and B. Smit, *Understanding Molecular Simulation: From Algorithms to Applications*, Computational Science Series (Elsevier Science, New York, 2001).
[38] M. Praprotnik, L. Delle Site, and K. Kremer, J. Chem. Phys. **123**, 224106 (2005).
[39] J. D. Halverson, T. Brandes, O. Lenz, A. Arnold, S. Bevc, V. Starchenko, K. Kremer, T. Stuehn, and D. Reith, Comput. Phys. Commun. **184**, 1129 (2013).
[40] A. Stukowski, Model. Simul. Mater. Sci. Eng. **18**, 015012 (2010).
[41] See Supplemental Material at http://link.aps.org/supplemental/10.1103/PhysRevLett.118.055702 for further details on the simulation setup and the performed analysis, which includes Refs. [42–46].
[42] J. S. Rowlinson and F. Swinton, *Liquids and Liquid Mixtures: Butterworths Monographs in Chemistry* (Butterworth-Heinemann, London, 2013).
[43] H. J. C. Berendsen, J. P. M. Postma, W. F. van Gunsteren, A. DiNola, and J. R. Haak, J. Chem. Phys. **81**, 3684 (1984).
[44] P. H. Hünenberger, in *Advanced Computer Simulation: Approaches for Soft Matter Sciences I* (Springer, Berlin, Heidelberg, 2005) Chap. 2, p. 105.
[45] P. R. ten Wolde, M. J. Ruiz-Montero, and D. Frenkel, Phys. Rev. Lett. **75**, 2714 (1995).
[46] H.-J. Zhang, S.-M. Peng, X.-S. Zhou, and X. Ju, Europhys. Lett. **107**, 46002 (2014).
[47] M. H. Lamm and C. K. Hall, AIChE J. **47**, 1664 (2001).
[48] G. C. McNeil-Watson and N. B. Wilding, J. Chem. Phys. **124**, 064504 (2006).
[49] P. J. Steinhardt, D. R. Nelson, and M. Ronchetti, Phys. Rev. B **28**, 784 (1983).
[50] H. E. A. Huitema, M. J. Vlot, and J. P. van der Eerden, J. Chem. Phys. **111**, 4714 (1999).
[51] H. E. A. Huitema, B. van Hengstum, and J. P. van der Eerden, J. Chem. Phys. **111**, 10248 (1999).
[52] J. Thomson, *The London, Edinburgh and Dublin Philosophical Magazine and Journal of Science* (Taylor & Francis, London, 1871).

[53] J. Thomson, *Applications of Dynamics to Physics and Chemistry* (Macmillan, London, 1888).
[54] J. Gibbs, H. Bumstead, and R. Van Name, *Scientific Papers of J. Willard Gibbs ...*, Scientific Papers of J. Willard Gibbs (Longmans, Green, New York, 1906).
[55] A. Widmer-Cooper and P. Harrowell, J. Chem. Phys. **126**, 154503 (2007).
[56] A. Guinier and G. Fournet, *Small-angle scattering of X-rays* (Wiley, New York, 1955).
[57] A. Pagnani and G. Parisi, Phys. Rev. E **92**, 010101 (2015).
[58] Q. Shi and T. Cai, Cryst. Growth Des. **16**, 3279 (2016).